Magnetism in Mn-nanowires and -clusters as δ-doped layers in group IV semiconductors (Si, Ge)

K. R. Simov, P.-A. Glans, C. A. Jenkins, M. Liberati, and P. Reinke

Citation: APL Materials **6**, 016105 (2018); doi: 10.1063/1.4996299
View online: https://doi.org/10.1063/1.4996299
View Table of Contents: http://aip.scitation.org/toc/apm/6/1
Published by the American Institute of Physics

Magnetism in Mn-nanowires and -clusters as δ-doped layers in group IV semiconductors (Si, Ge)

K. R. Simov,[1] P.-A. Glans,[2] C. A. Jenkins,[2] M. Liberati,[2] and P. Reinke[1]
[1]*Department of Materials Science and Engineering, University of Virginia, 395 McCormick Road, Charlottesville, Virginia 22901, USA*
[2]*Advanced Light Source, Lawrence Berkeley National Laboratory, Berkeley, California 94720, USA*

(Received 15 July 2017; accepted 11 December 2017; published online 18 January 2018)

Mn doping of group-IV semiconductors (Si/Ge) is achieved by embedding nanostructured Mn-layers in group-IV matrix. The Mn-nanostructures are monoatomic Mn-wires or Mn-clusters and capped with an amorphous Si or Ge layer. The precise fabrication of δ-doped Mn-layers is combined with element-specific detection of the magnetic signature with x-ray magnetic circular dichroism. The largest moment (2.5 μ_B/Mn) is measured for Mn-wires with ionic bonding character and a-Ge overlayer cap; a-Si capping reduces the moment due to variations of bonding in agreement with theoretical predictions. The moments in δ-doped layers dominated by clusters is quenched with an antiferromagnetic component from Mn–Mn bonding. https://doi.org/10.1063/1.4996299

The success of spintronics, which uses the electron spin for device operation,[1–4] hinges on development of materials offering exquisite control of magnetism and spin current. One of the central challenges in the study and use of dilute magnetic semiconductors (SC) is merging spin-controlled and charge-based devices. This can be achieved with magnetically doped SCs[2,5] where the magnetic response can be controlled via an electric field. Mn is a prime candidate for magnetic doping and has been used successfully in GaAs(Mn)[6,7] and was proposed as a magnetic dopant in the group-IV SCs, Si and Ge.[3,8–13] The inherent complexity of the Mn–Si and Mn–Ge material systems owing to the coexistence of interstitial and substitutional sites, clusters, and compounds has generally impeded our understanding of magnetism in these systems.

The wide range of magnetic properties reported in the literature for Mn-doped group IV SCs[8,11–17] suggest that we lack control and understanding of critical material aspects and how they control magnetic signatures. Recent work on Mn-ion implantation in Si illustrates the complex interplay between different coordination sites and defect chemistries which have to be considered in the investigation of magnetically doped semiconductors.[18] In addition, the formation of silicides and germanides and a wide range of metastable materials residing in the Ge (or Si) rich region of the phase diagram[12,15,17] prevent precise control of material structure, which is necessary to understand the connection between bonding environment and magnetism. We therefore use δ-doped layers, which are self-assembled Mn-nanostructures embedded in a group IV semiconductor matrix[19–24] and afford excellent control of the Mn-bonding environment.

Our work combines the synthesis of well-defined nanostructures of Mn on Si(001) and element-specific detection of the magnetic signature of Mn with XMCD (x-ray magnetic circular dichroism). Mn is deposited on Si(100)-(2 × 1) surfaces, which serve as a template for monoatomic Mn-wires, and Mn-clusters.[19,21–23,25] These Mn-nanostructures are characterized with STM (scanning tunneling microscopy) and subsequently capped with an amorphous Si or Ge layer. The capping process preserves the respective Mn-nanostructures and creates a δ-doped Mn-layer as confirmed with angle-dependent XAS (x-ray absorption spectroscopy) measurements in our work, and in agreement with the literature.[24] This approach enables us to modulate the Mn-atom nearest neighbor environment

and directly correlate with the magnetic signature. Our study connects the Mn–Si bonding with the Si(001)-(2 × 1) surface and the amorphous cap to the magnetic signature of δ-doped structures.

Monoatomic Mn-wires shown in Fig. 1 self-assemble on the Si(001)-(2 × 1) reconstruction and nucleate preferentially at C-type defects sites.[21,22] The end of the growing wire is a preferred attachment site for Mn atoms—fewer defects in the Si(100) surface will yield longer wires up to a length of 20-30 nm. Annealing leads to a disintegration of the wires and formation of silicides by a solid state reaction.[20] The bonding between nanowires and the Si surface is best described by a recent model,[23] where the Mn atoms are integrated in the Si-dimer leading to Mn-wires running perpendicular to the Si-dimer rows with an interatomic Mn–Mn distance of 0.85 nm. According to the Bethe-Slater curve, this should yield ferromagnetic coupling within the wire but neglects the Mn–Si interaction. Ultrasmall Mn-clusters are obtained if the defect concentration on the Si(001)-(2 × 1) surface is above 5%.[22]

Figure 1 shows STM images for all nanostructures used in the present study, and Fig. 1(a) is a high resolution image showing the details of the Mn-wire and Si-dimer row surface. The wire quality[22] was defined previously as the surface area covered by Mn-wires divided by the total area covered by wires and clusters, and a surface covered predominantly by wires is therefore termed a "high quality" nanostructure.[20,21] The material used for the XMCD experiments includes high quality wires in Figs. 1(a), 1(b), and 1(d), mixed nanostructures with a sizable contribution from clusters in Figs. 1(c) and 1(e), and Mn layers with a thickness of 2 ML, where clusters dominate [Fig. 1(e)]. All STM images were recorded at room temperature using an etched W-tip with a bias voltage of 1.6 V and a feedback current of 0.05 nA.[21,22] All images shown in Fig. 1 are recorded for samples used in the subsequent XAS/XMCD/XMLD analysis.

Mn-deposition on Si(001) and the subsequent growth of a Si or Ge capping layer to form the δ-doped layers, were performed in an ultrahigh-vacuum preparation chamber connected to an Omicron VT-STM (variable temperature scanning tunneling microscope). The Si surface was cleaned by annealing-flashing cycles.[26] Mn and Si are evaporated using an e-beam evaporator (Mantis) with a rate of about 6.5×10^{-3} ML/s. One ML Mn corresponds to 1.15×10^{15} atoms/cm^2, and rates are calibrated with a quartz crystal monitor. Ge is evaporated from a VEECO effusion cell at about

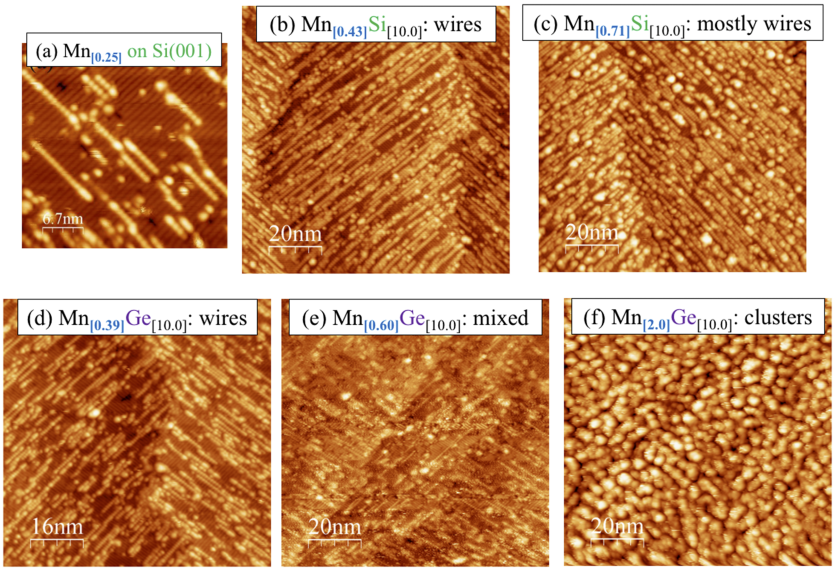

FIG. 1. STM images of the Mn-nanostructures, and (a) shows a typical image of the Mn-wires for a coverage of 0.25 ML Mn. This sample was not used in the XMCD experiments and the low coverage allows better visibility of the wires and Si-surface. All other images show samples which were used after capping in the XMCD analysis. Mn self-assembles on the Si(001)-(2 × 1) surface into wires (b) and (d), mostly wires with few clusters (c) and (e), and only clusters for coverages exceeding 1 ML (f). Details of the wire formation, atomic scale structure, and interplay between wire and cluster formation are given in Refs. 20–22. The top row samples [(b) and (c)] were capped with an amorphous Si layer with a thickness of 10 ML, and bottom row samples [(d)–(f)] were capped with an amorphous Ge layer.

0.04 ML/s. The Mn-nanostructure and capping layer growth are finalized within three hours. However, the Mn-nanostructures prior to capping are stable for considerably longer time periods exceeding a full day of STM measurements. The Mn XAS spectra of the capped nanostructures do not show any Mn-oxides, which is confirmed by comparison with the literature.[10,11] All depositions are performed at room temperature, which yields amorphous capping layers with a thickness of 10 ML. At intermittent steps in the early stages of capping layer growth, STM measurements were performed to verify that the Mn nanostructures are preserved. The Mn-wires and Mn-clusters can be distinguished from the Ge or Si deposit due to a unique contrast variation as a function of bias voltage.[27] The individual samples are labeled as the following: the subscript gives the respective layer thickness in ML (monolayer) and the second element indicates the capping layer material, e.g., $Mn_{[0.43]}Si_{[10]}$. Angle-resolved XAS measurements were performed after transport of the samples to the advanced light source and show that the Mn-signal attenuation follows the Lambert-Beer law which confirms the stability of the δ-doped Mn-layer in agreement with Ref. 24. The Mn-coverage can therefore be used to calculate the magnetic moments.[28]

XAS, XMCD, and x-ray magnetic linear dichroism (XMLD) were used to study the electronic and magnetic properties of the embedded Mn nanostructures.[29] The measurements were carried out at beamline 6.3.1 of the Advanced Light Source, and only $Mn_{[0.6]}Ge_{[10]}$ was measured at beamline 4.0.2. The $L_{3,2}$ Mn peaks were recorded in the photon energy range from 630 to 660 eV. A saturation **B**-field of 2 T was applied parallel to the incident x-ray beam and XAS spectra were collected for +/− polarity of the field with respect to the beam direction in the total electron yield mode. The dichroism signal is obtained by switching the **B**-field direction, and the magnetic alignment is confirmed by inverting the x-ray polarization. A gold mesh with +250 V bias voltage was used to remove contributions from spurious secondary electrons. The small Mn inventory in our samples and the presence of the capping layer required exceptionally long data acquisition times (>12 h per sample) to achieve a reasonable signal-to-noise ratio. Due to the very long acquisition times, the sample temperatures are between 20 and 50 K but were constant within each measurement. The dichroism signal is extracted from XAS spectra measured with opposing magnetic saturation fields after matching the intensity at the L_3 pre-edge position and then analyzed using the sum rules established by Chen *et al.*[30] The spectra were corrected for measurement geometry, and the number of holes is adjusted at 4.52 following band structure calculations.[31] XMLD spectra were measured with linearly polarized light in the same geometry. VSM (vibrating sample magnetometry) measurements were performed, but the signal-to-noise ratio is poor due to the small Mn inventory and the large contribution from the diamagnetic Si-wafer. The same challenges are encountered in superconducting quantum interference device (SQUID) measurements, and element-specific magnetism measurements with XMCD are therefore best suited to study this material system. The magnetic moments derived from the hysteresis loops agreed within 30% of the XMCD data; the lowest Mn concentrations did not yield VSM data. The Curie temperature (T_{Curie}) is between 70 and 100 K.

The XAS spectra summarized in Fig. 2 have an L_3 peak (638 eV) with two shoulders on the high energy side (639.5 and 641 eV) and an L_2 peak doublet at 648 and 650 eV. Peak shapes and positions show little variations across all samples and are in agreement with a predominantly Mn^{2+} (d^5) bonding state.[10,32] The difference between tetrahedrally and octahedrally coordinated Mn^{2+} is small,[33] and our resolution did not allow us to distinguish between them. The peak shape and positions, and specifically the shape of the L_3 pre-edge region, are clearly distinct from Mn-oxides with d^3 to d^5 configurations. Mn thin films and Mn-doped a-Si (Mn > 0.5 at. %), on the other hand, exhibit significant spectral broadening of the L_3 and L_2 peaks, which is due to electron delocalization in the Mn-metal and a 3d-impurity band for the Mn-doped material, respectively.[10] Even the thickest δ-doped Mn-layer with 2 ML equivalent coverage, which consists of "pancake shaped" clusters, does not display metallic behavior. The ionic signature from the hybridization of Mn-3d band with Si-substrate and capping layer dominates the spectral signature. In a weighted superposition of metal and ionic XAS spectra (Mn^{2+} d^5, a-Mn_xGe_{1-x} for x = 0.05),[10] the overall spectral signature will only visibly change if the metallic contribution exceeds 30%, a limit not reached in our experiment.

The magnetic moments for all samples are shown in Fig. 3 and summarized in Table I, which also includes the orbital and spin contributions extracted from the XMCD spectra shown in Fig. 3. In the majority of samples, M_{spin} dominates and the orbital contributions tend to be small. The highest

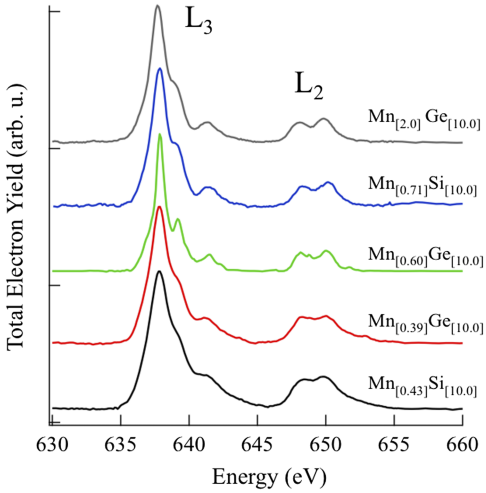

FIG. 2. XAS spectra of the $L_{3,2}$ Mn edge for all samples shown in Fig. 1. Sample $Mn_{[0.6]}Ge_{[10.0]}$ was measured at beamline 4.0.2 with a higher energy resolution leading to narrower features in the spectrum. The $L_{3,2}$ intensity as a function of take-off angle for $Mn_{[0.71]}Si_{[10.0]}$ and $Mn_{[2.0]}Ge_{[10.0]}$ follows the Lambert-Beer law if a buried Mn layer is assumed with no Mn contribution within the capping layer or at the surface.

M_{total} is observed for the best nanowire structures: $Mn_{[0.43]}Si_{[10]}$, $Mn_{[0.39]}Ge_{[10]}$, and $Mn_{[0.71]}Si_{[10]}$, while clustering significantly lowers M_{total}. In addition, M_{total} given in moment/atom is identical for $Mn_{[0.43]}Si_{[10]}$ and $Mn_{[0.71]}Si_{[10]}$, both of which have predominantly Mn-nanowires [Figs. 1(a) and 1(b)]. The magnetic signature of the nanowires falls in line with the theoretical predictions for Mn-adatoms on Si(001) surfaces, which yield between 2.0 and 4.1 μ_B/Mn for different Mn-bonding geometries. The configuration which is closest to the experimental Mn-wire structure (bonding site

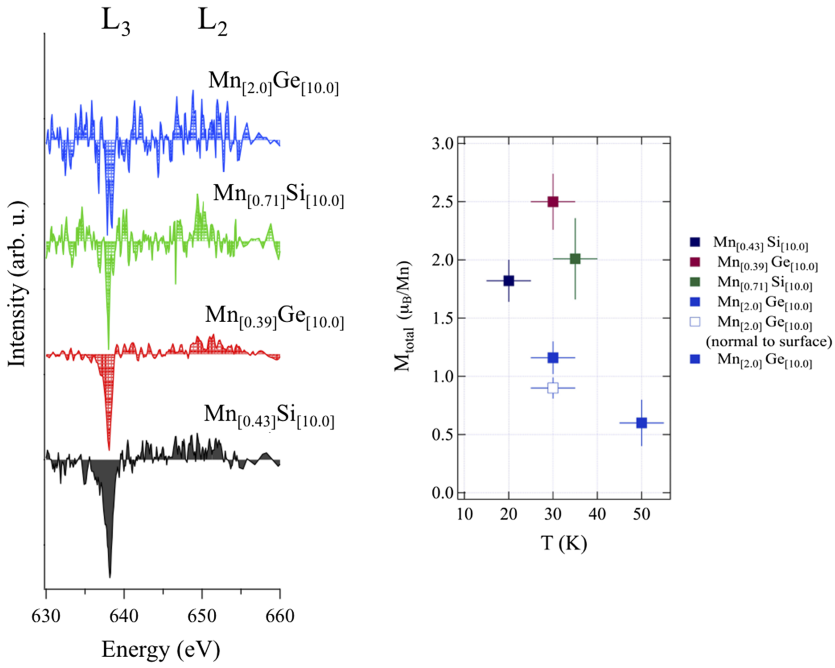

FIG. 3. XMCD spectra for the L_3 Mn peak for the samples shown in Fig. 1. The moment M_{total} for all samples is summarized in the graph on the right-hand side. The values for the spin and orbital moments are summarized in detail in Table I. The small Mn inventory combined with attenuation of the signal due to the capping layer contributes to the relatively high noise in the dichroism spectra, which is taken into account in the error bar included in M_{total}.

TABLE I. Summary of magnetic moments calculated from XMCD spectra using the sum rules. The sample compositions are given in the first column, and the nanostructure type, temperature, and angle to the surface normal are summarized in the "Comment" column. M_{orb} is the magnetic orbital moment, M_{spin} is the spin moment, and their sum, the total magnetic moment M_{total} is shown in Fig. 3(b). $Mn_{[2.0]}Ge_{[10.0]}$ is the only sample where XMCD spectra could be obtained for two different angles given with respect to the substrate normal.

Composition	Mn nanostructure type; T during measurement (K); angle to surface normal°	M_{orb} (μ_B/Mn)	M_{spin} (μ_B/Mn)	M_{total} (μ_B/Mn)
(a) $Mn_{[0.43]}Si_{[10.0]}$	Wires T = 20 K, 60°	0.20 ± 0.04	1.62 ± 0.11	1.82 ± 0.18
(b) $Mn_{[0.39]}Ge_{[10.0]}$	Wires T = 30 K, 60°	0.02 ± 0.02	2.48 ± 0.21	2.50 ± 0.24
(c) $Mn_{[0.71]}Si_{[10.0]}$	Mostly wires T = 35 K, 60°	0.06 ± 0.01	1.95 ± 0.31	2.01 ± 0.35
(d) $Mn_{[0.6]}Ge_{[10.0]}$	Mixed	Only XAS available		
(e1) $Mn_{[2.0]}Ge_{[10.0]}$	Clusters T = 30 K, 60°	0.01 ± 0.01	1.15 ± 0.12	1.16 ± 0.14
(e2) $Mn_{[2.0]}Ge_{[10.0]}$	Clusters T = 30 K, 0°	0.09 ± 0.02	0.81 ± 0.07	0.90 ± 0.09

"H" as defined in Ref. 8) and has a moment of 3.2 μ_B/Mn. A hybridization between the Mn-nanowire atoms (localized 3d-state) with the Si-p and s-bands stabilizes the ferromagnetic (FM) coupling. The reduced moment for mixed and Mn-cluster rich layers can be attributed to increasing contributions of direct Mn–Mn bonding, which adds an antiferromagnetic (AFM) component leading to overall reduction in M_{total}. In addition, M_{total} has already decreased significantly at 50 K indicating a relatively low T_{Curie}. XMLD spectra, which reflect antiferromagnetic coupling, support this interpretation.[34] The intensity of L_3 peak in the XMLD spectra correlates with the contributions from Mn-clusters relative to Mn-nanowires: the highest intensity in L_3 of the XMLD spectra is seen for $Mn_{[2.0]}Ge_{[10]}$ where the XMCD signal already is relatively small and the XMLD signal disappears for $Mn_{[0.43]}Si_{[10]}$, $Mn_{[0.39]}Ge_{[10]}$ Despite their relatively poor signal-to-noise ratio, XMLD spectra support an increasing AFM component for samples rich in Mn-clusters.

The choice of capping layer, a-Si and a-Ge, has also a sizeable impact on the magnetic signature of the δ-doped Mn-layers. M_{total} is larger for samples with an a-Ge cap despite the slightly higher measurement temperature for $Mn_{[0.39]}Ge_{[10]}$ compared to $Mn_{[0.41]}Si_{[10]}$. The latter is the only sample with a sizeable M_{orb}, whose origin is currently not understood. The position of the Mn-atoms is fixed by the Si(001) substrate, but the number of nearest neighbors will be lower for Ge than for Si. The correlation between the moment at the Mn atom and the number of nearest neighbors has been studied for amorphous Si–Mn and Ge–Mn materials[10] and can be traced back to the differences in the density of states of the two spin channels, which is in turn controlled by the hybridization between SC and Mn states. A larger number of nearest neighbors will lead to a partial quenching of the local Mn moments, which is commensurate with our observation of a lower moment for the a-Si-cap. The complete quenching of the Mn moments and transition to a metallic signature in XAS, which has been observed for a-Si:Mn, is prevented for the nanowires by bonding to the Si(001) surface.

In low-dimensional systems, the spin-orbital coupling defines the orientation of the easy magnetic axis.[35,36] In ultrathin transition metal thin films such as Co embedded in Au,[36] the easy axis can be oriented out of plane due to the spin orbit coupling and associated magnetocrystalline anisotropy. This overrides the shape anisotropy which favors the alignment of the moment within the plane of the magnetic layer. Measuring M_{orb} for two angles in $Mn_{[2.0]}Ge_{[10.0]}$ yields 0.09 ± 0.02 μ_B/Mn for the normal direction and 0.01 ± 0.02 μ_B/Mn for 60° with respect to the normal, which is our customary measurement geometry. This is commensurate with a larger spin-orbit coupling and easy axis in the out-of-plane direction. Consequently, the easy magnetic axis is in-plane for the $Mn_{[2.0]}Ge_{[10.0]}$ clustered sample. The majority of our samples shows a very small M_{orb} for 60° and thus might also prefer the out-of-plane easy axis. However, this analysis should be taken with a grain of salt due to the overall small values of the orbital moment and limited number of data points.

The combination of atomic level control in the synthesis of magnetic nanostructures and element-specific measurements of magnetic properties yields a new level of understanding in the magnetic doping of group IV semiconductors. In conclusion, we demonstrated the ferromagnetic coupling between Mn-atoms organized within monoatomic chains on the Si(001) surface, although the Curie temperatures remain relatively low. The antiferromagnetic Mn–Mn interaction, which is

present in Mn-nanoclusters, depresses M_{total} and confirms that any clustering will diminish magnetic performance of a doped semiconductor. It is also quite remarkable that the impact of the capping layer material is evident in our data and shows that careful selection of capping layer material can enhance performance. Overall this work illustrates clearly that the unusual combination of STM and XMCD performed for the same sample is a powerful method for interpreting and understanding magnetism in nanostructures.

The authors gratefully acknowledge the support of this work by the NSF with Award No. DMR-0907234, Division of Materials Research (Electronic and Photonic Materials). This work was only possible in collaboration with the scientists and excellent facilities at the Advanced Light Source. The Advanced Light Source is supported by the Director, Office of Science, Office of Basic Energy Sciences, the U.S. Department of Energy under Contract No. DE-AC02-05CH11231.

[1] D. Awschalom and M. E. Flatte, "Challenges for semiconductor spintronics," Nat. Phys. **3**, 153 (2007).
[2] T. Dietl and H. Ohno, "Dilute ferromagnetic semiconductors: Physics and spintronic structures," Rev. Mod. Phys. **86**, 187–251 (2014).
[3] T. Dietl, K. Sato, T. Fukushima, A. Bonanni, M. Jamet, A. Barski, S. Kuroda, M. Tanaka, P. N. Hai, and H. Katayama-Yoshida, "Spinodal nanodecomposition in semiconductors doped with transition metals," Rev. Mod. Phys. **87**, 1311–1377 (2015).
[4] I. Žutić, J. Fabian, and S. D. Sarma, "Spintronics: Fundamentals and Applications," Rev. Mod. Phys. **76**, 323 (2004)
[5] H. Ohno, "Making non-magnetic semiconductors ferromagnetic," Science **281**, 951 (1998).
[6] K. Olejnik, P. Wadley, J. A. Haigh, K. W. Edmonds, R. P. Campion, A. W. Rushforth, B. L. Gallagher, C. T. Foxon, T. Jungwirth, J. Wunderlich, S. S. Dhesi, S. A. Cavill, G. van der Laan, and E. Arenholz, "Exchange bias in a ferromagnetic semiconductor induced by a ferromagnetic metal: Fe/(Ga,Mn)As bilayer films studied by XMCD measurements and SQUID magnetometry," Phys. Rev. B **81**, 104402 (2010).
[7] M. Wang, R. P. Campion, A. W. Rushforth, K. W. Edmonds, C. T. Foxon, and B. L. Gallagher, "Achieving high Curie temperature in (Ga, Mn)As," Appl. Phys. Lett. **93**, 132103 (2008).
[8] M. Hortamani, H. Wu, P. Kratzer, and M. Scheffler, "Epitaxy of Mn on Si(001): Adsorption, surface diffusion, and magnetic properties studied by density-functional theory," Phys. Rev. B **74**, 205305 (2006).
[9] H. Wu, P. Kratzer, and M. Scheffler, "Density-functional theory study of half-metallic heterostructures: Interstitial Mn in Si," Phys. Rev. Lett. **98**, 117202 (2007).
[10] L. Zeng, J. X. Cao, E. Helgren, J. Karel, E. Arenholz, L. Ouyang, D. J. Smith, R. Q. Wu, and F. Hellman, "Distinct local electronic structure and magnetism for Mn in amorphous Si and Ge," Phys. Rev. B **82**, 165202 (2010).
[11] S. Tardif, A. Titov, E. Arras, I. Slipukhina, E.-K. Hlil, S. Cherifi, Y. Joly, M. Jamet, A. Barski, J. Cibert, E. Kulatov, Y. A. Uspenskii, and P. Pochet, "X-ray magnetic circular dichroism in (Ge,Mn) compounds: Experiments and modeling," J. Magn. Magn. Mater. **354**, 151–158 (2014).
[12] P. Gambardella, L. Claude, S. Rusponi, K. J. Franke, H. Brune, J. Raabe, F. Nolting, P. Bencok, A. T. Hanbicki, B. T. Jonker, C. Grazioli, M. Veronese, and C. Carbone, "Surface characterization of Mn_xGe_{1-x} and $Cr_yMn_xGe_{1-x-y}$ dilute magnetic semiconductors," Phys. Rev. B **75**, 125211 (2007).
[13] Y. D. Park, A. T. Hanbicki, S. C. Erwin, C. S. Hellberg, J. M. Sullivan, H. E. Mattson, T. F. Ambrose, A. Wilson, G. Spanos, and B. T. Jonker, "A group-IV ferromagnetic semiconductor: $MnxGe_{1-x}$," Science **295**, 651 (2002).
[14] S. Ahlers, P. R. Stone, N. Sircar, E. Arenholz, O. D. Dubon, and D. Bougeard, "Comparison of the magnetic properties of GeMn thin films through Mn L-edge x-ray absorption," Appl. Phys. Lett. **95**, 151911 (2009).
[15] M. Jamet, A. Barski, T. Devillers, V. Poydenot, R. Dujardin, P. Bayle-Guillemaud, J. Rothman, E. Bellet-Amalric, A. Marty, J. Cibert, R. Mattana, and S. Tatarenko, "High-Curie-temperature ferromagnetism in self-organized $Ge_{1-x}Mn_x$ nanocolumns," Nat. Mater. **5**, 653–659 (2006).
[16] J. S. Kang, G. Kim, S. C. Wi, S. S. Lee, S. Choi, S. Cho, S. W. Han, K. H. Kim, H. J. Song, H. J. Shin, A. Sekiyama, S. Kasai, S. Suga, and B. I. Min, "Spatial chemical inhomogeneity and local electronic structure of Mn-doped Ge ferromagnetic semiconductors," Phys. Rev. Lett. **94**, 147202 (2005).
[17] J. Kassim, C. Nolph, M. Jamet, P. Reinke, and J. Floro, "$Ge_{1-x}Mn_x$ heteroepitaxial quantum dots: Growth, morphology, and magnetism," J. Appl. Phys. **113**, 073910 (2013).
[18] D. J. da Silva, U. Wahl, J. G. Correia, L. M. Amorim, S. Decoster, M. R. da Silva, L. M. D. C. Pereira, and J. P. Araújo, "Direct observation of the lattice sites of implanted manganese in silicon," Appl. Phys. A **122**, 241 (2016).
[19] A. Fuhrer, F. J. Ruess, N. Moll, A. Curioni, and D. Widmer, "Atomic structure of Mn wires on Si(001) resolved by scanning tunneling microscopy," Phys. Rev. Lett. **109**, 146102 (2012).
[20] C. Nolph, K. R. Simov, H. Liu, and P. Reinke, "Manganese nanostructures on Si(100)(2x1) surfaces: Temperature driven transition from wires to silicides," J. Phys. Chem. C **114**, 19727 (2010).
[21] C. A. Nolph, H. Liu, and P. Reinke, "Bonding geometry of Mn-wires on the Si(100)(2 × 1) surface," Surf. Sci. **605**, L29–L32 (2011).
[22] K. R. Simov, C. A. Nolph, and P. Reinke, "Guided self-assembly of Mn wires on the Si(100)(2 × 1) surface," J. Phys. Chem. C **116**, 1670–1678 (2012).
[23] R. Villarreal, M. Longobardi, S. A. Koster, Ch. J. Kirkham, D. Bowler, and C. Renner, "Structure of self-assembled Mn atom chains on Si(001)," Phys. Rev. Lett. **115**, 256104 (2015).
[24] F. J. Rueß, M. El Kazzi, L. Czornomaz, P. Mensch, M. Hopstaken, and A. Fuhrer, "Confinement and integration of magnetic impurities in silicon," Appl. Phys. Lett. **102**, 082101 (2013).

[25] D. R. Bowler, "Atomic-scale nanowires: Physical and electronic structure," J. Phys.: Condens. Matter **16**, R721–R754 (2004).
[26] K. Hata, T. Kimura, S. Ozawa, and H. Shigekawa, J. Vac. Sci. Technol., A **18**, 1933 (2000).
[27] K. R. Simov, "Manganese nanostructures and magnetism," Ph.D. thesis, University of Virginia, 2011, available at: https://search.lib.virginia.edu/catalog/u5576186.
[28] K. W. Edmonds, N. R. S. Farley, R. P. Campion, C. T. Foxon, B. L. Gallagher, T. K. Johal, G. van der Laan, M. MacKenzie, J. N. Chapman, and E. Arenholz, "Surface effects in Mn L3,2 x-ray absorption spectra from (Ga,Mn)As," Appl. Phys. Lett. **84**, 4065–4067 (2004).
[29] J. Stöhr, J. Magn. Magn. Mater. **200**, 470 (1999).
[30] C. T. Chen, Y. U. Idzerda, H.-J. Lin, N. V. Smith, G. Meigs, E. Chaban, G. H. Ho, E. Pellegrin, and F. Sette, Phys. Rev. Lett. **75**, 152 (1995).
[31] J. Schmalhorst, S. Kaemmerer, M. Sacher, G. Reiss, A. Huetten, and A. Scholl, Phys. Rev. B **70**, 024426 (2004).
[32] L. Zeng, A. Huegel, E. Helgren, F. Hellman, C. Piamonteze, and E. Arenholz, "X-ray absorption study of the electronic structure of Mn-doped amorphous Si," Appl. Phys. Lett. **92**, 142503 (2008).
[33] G. V. D. Laan and I. W. Kirkman, "The 2p absorption spectra of 3d transition metal compounds in tetrahedral and octahedral symmetry," J. Phys.: Condens. Matter **4**, 4189 (1992)
[34] A. Scholl, M. Liberati, E. Arenholz, H. Ohldag, and J. Stohr, "Creation of an antiferromagnetic exchange spring," Phys. Rev. Lett. **92**, 247201 (2004).
[35] P. Gambardella, A. Dallmeyer, K. Maiti, M. C. Malagoli, S. Rusponi, P. Ohresser, W. Eberhardt, C. Carbone, and K. Kern, "Oscillatory magnetic anisotropy in one-dimensional atomic wires," Phys. Rev. Lett. **93**, 077203 (2004).
[36] D. Weller, J. Stohr, R. Nakajima, A. Carl, M. G. Samant, C. Chappert, R. Megy, P. Beauvillain, P. Veillet, and G. A. Held, "Microscopic origin of magnetic anisotropy in Au/Co/Au probed with x-ray magnetic circular dichroism," Phys. Rev. Lett. **75**, 3752–3755 (1995).